$[Fe^{III}(tmdta)]^-$–twist-boat/half-chair conformer ratio reliably deduced from DFT-calculated Raman spectra†

Roland Meier,*[a] Joachim Maigut,[a] Bernd Kallies,*[b] Nicolai Lehnert,*[c] Florian Paulat,[c] Frank W. Heinemann,[a] Gernot Zahn,[d] Martin P. Feth,[e] Harald Krautscheid[f] and Rudi van Eldik[a]

Received (in Cambridge, UK) 4th June 2007, Accepted 10th August 2007
First published as an Advance Article on the web 20th August 2007
DOI: 10.1039/b708437d

The equilibrium between the twist-boat (tb) and half-chair (hc) conformers of the central diamine chelate ring of $[Fe^{III}(tmdta)]^-$ in solids and aqueous solution has been studied by Raman spectroscopy, supported by calculated Raman spectra using Density Functional Theory.

Monitoring changes in the coordination sphere around iron centers that result from the dissolution of solid complex salts in water is of high importance for the elucidation of structure–activity relationships,[1] a critical target in many industrial and academic applications of iron chelates.[2] The complex investigated here, $[Fe^{III}(tmdta)]^-$ (tmdta = trimethylenediamine tetraacetate), is used in the bleaching of photographic films and paper.[3] The conformational equilibria of chelate complexes are often very difficult to monitor, especially in the cases of complexes with paramagnetic metal centers. Here, the use of NMR for structural elucidation fails. In this study, we demonstrate how Raman spectroscopy coupled to density functional theory (DFT) calculations can be successfully applied for this purpose.

Upon coordination to tmdta, metal centers like Fe^{III} can form half-chair (**hc**) or twist-boat (**tb**) conformational isomers (see Scheme 1).[4–6] The half-chair conformer was found in the crystal structure of $Li[Fe(tmdta)]\cdot 3H_2O$ (**1a**),[3] whereas the twist-boat form was encountered during structural studies of $NH_4[Fe(tmdta)]\cdot H_2O$ (**1b**)[4] and $Na[Fe(tmdta)]\cdot 3H_2O$ (**1c**).[5]

Various salts of $[Fe^{III}(tmdta)]^-$ have been studied in the past by solid-state Raman spectroscopy,[7] followed by the analysis of the Raman spectra of their corresponding aqueous solutions.[8] In the latter study, the predominance of the **hc** form in solution was suggested, based on the evaluation of bands in the 600–300 cm^{-1} wavenumber region. Here, Fe–N and Fe–O valence stretching, as well as skeletal vibrations of the coordination polyhedron, are expected to appear.[7,8] However, this analysis remained on an empirical level and was strongly impaired by the fact that the vibrational assignments of the bands used to identify the species found in solution were not known.

A major revision of these findings is presented in the current Communication. We have re-investigated the solid-state Raman spectra of the two isomers of $[Fe^{III}(tmdta)]^-$ in detail and correlated the experimental data to Raman spectra calculated by DFT. For this purpose, the structures of the two conformers were fully optimized in the gas phase using B3LYP/6-31+G* (*cf.* Computational aspects in the ESI†). The computed spectra were then used to simulate the composite spectra of conformer mixtures, which were correlated to the experimental Raman spectra of aqueous solutions of $[Fe^{III}(tmdta)]^-$ salts.

In the structural studies reported to date,[4–6] it was not clearly determined which of the two conformers (**tb** or **hc**) was preferred in the solid-state. In order to broaden the knowledge basis for this purpose, we have investigated the crystal structures of two new Fe^{III}–tmdta salts, *i.e.* $K[Fe^{III}(tmdta)]$ (**1d**) and $\{C(NH_2)_3\}[Fe^{III}(tmdta)]\cdot 2H_2O$ (**1e**).‡ In both cases, the **tb** conformation is found in the solid-state. Interestingly, the structure of **1e** also contains 6% of the **hc** conformer, leading to disorder in the crystal (further details are presented in the ESI†). The latter finding motivated us to re-determine the structures of $Li[Fe^{III}(tmdta)]\cdot 3H_2O$ (**1a**)[4] and $NH_4[Fe^{III}(tmdta)]\cdot 0.5H_2O$ (**1b**) at high resolution in order to explore the possibility of conformational mixtures in these salts.§[5] From the literature, fractional coordinates are available for **1a**.[4] This is not the case for **1b**, where only the lattice constants have been published.[5] It was again surprising that—while **1b** contains solely the **tb** form—salt **1a**, which was originally considered to be purely **hc**, in fact shows a similar disorder to that encountered for **1e**, but with a distribution of 91% **hc** *vs.* 9% **tb**. Our results now show rather clearly that the **tb**

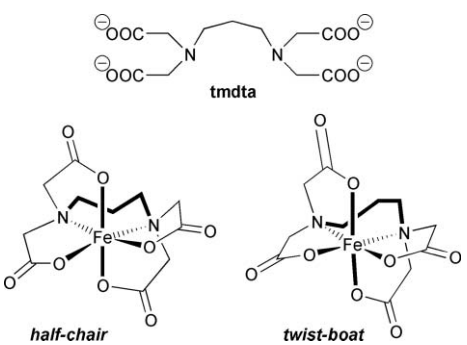

Scheme 1 The ligand tmdta, and the half-chair and twist-boat conformational isomers of $[Fe^{III}(tmdta)]^-$.

[a]*Institute for Inorganic Chemistry, University of Erlangen-Nürnberg, Egerlandstraße 1, 91058 Erlangen, Germany*
[b]*Zuse Institute Berlin, Takustraße 7, 14195 Berlin, Germany*
[c]*Department of Chemistry, The University of Michigan, 930 N. University, Ann Arbor, MI 48109-1055, USA*
[d]*MPI für Chemische Physik fester Stoffe, Nöthnitzer Straße 40, 01187 Dresden, Germany*
[e]*ALTANA Pharma AG, A Member of the NYCOMED Group, Physicochemical Research, Byk-Gulden-Straße 2, 78467 Konstanz, Germany*
[f]*Institute of Inorganic Chemistry, University of Leipzig, Johannisallee 29, 04103 Leipzig, Germany*

† Electronic supplementary information (ESI) available: Preparation of complexes, X-ray structure analysis and crystallographic details, Raman spectra details and computational aspects. See DOI: 10.1039/b708437d

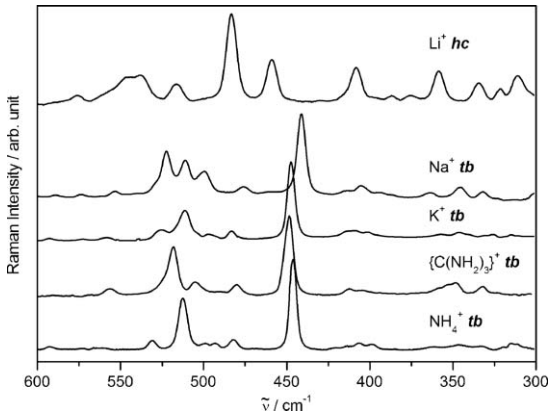

Fig. 1 Solid-state Raman spectra of $[Fe^{III}(tmdta)]^-$ salts **1a–e**. The counterion and dominating conformer found in the corresponding crystal structure (**hc** or **tb**) are indicated.

form is favoured in solid salts of $[Fe^{III}(tmdta)]^-$. Crystallization of the **hc** conformer seems only to be possible in the lithium salt.[9] However, one should take into account that the isomer distribution in the solid-state is a result of the counterbalancing solid-state forces in the crystal and does not reflect the intrinsic **tb** or **hc** arrangement characteristics of the metal complexes in the chelate backbone that is valid for solution- or gas-phase conditions.

As mentioned before,[8] in the 600–300 cm^{-1} wavenumber range, Fe–N and Fe–O valence stretching, as well as skeletal vibrations of

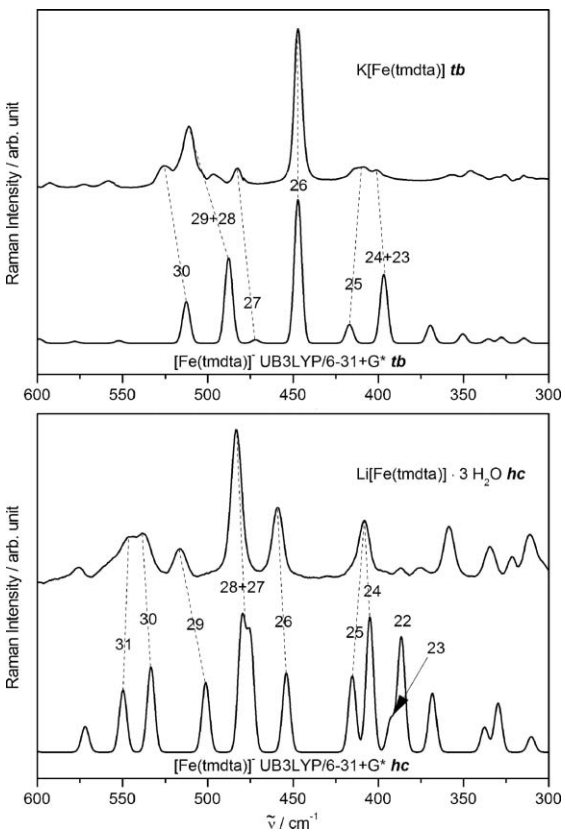

Fig. 2 Comparison of solid-state Raman spectra of the potassium (**1d**, top) and lithium (**1a**, bottom) salts of $[Fe^{III}(tmdta)]^-$ with calculated spectra of the twist-boat (top) and half-chair (bottom) conformers. Band numbering follows the entries in Table 1 and Table 2.

Table 1 Bands of the solid-state Raman spectrum of **1d** (**tb** conformer)

		Wavenumber/cm^{-1}			
No.	Sym.[a]	Exp'l[b]	Calc'd[c]	Intensity[d]	Description
23	A	401	396.3	11.8	Gly rock (eq.)
24	B		398.3	0.1	Gly rock (eq.)
25	B	409	416.5	3.2	Gly rock (all)
26	A	447	446.8	25.1	Ring twist
27	B	483	471.5	0.6	Gly rock (ax.)
28	B	511	485.5	2.1	ν_{as}(Fe–N)
29	A		487.5	13.3	ν_{s}(Fe–N)
30	A	525	512.2	7.1	Ring bend

[a] Irreducible representation in the C_2 point group. [b] *cf.* Fig. 2, top. [c] Calculated wavenumbers scaled by a factor of 1.027. [d] Calculated Raman intensity.

the coordination polyhedron, appear. Correspondingly, this is the most suitable wavenumber range to study the spectral differences between the **hc** and **tb** conformers. Thus, solid-state Raman spectra of the five salts, **1a–e**, of $[Fe^{III}(tmdta)]^-$ have been measured, as shown in Fig. 1 for the 600–300 cm^{-1} wavenumber range. The most prominent bands were assigned based on an analysis of the corresponding DFT-calculated spectra. These results are presented in Fig. 2, and in Table 1 and Table 2.

The most significant difference between the spectra of the two conformers is the presence of a very intense band at $\sim$440 cm^{-1} in all **tb** spectra, whereas the Raman intensity of the **hc** spectrum is virtually zero in this region (*cf.* Fig. 1). Our DFT computations show (*cf.* band 26 in Fig. 2 (top) and Table 1) that this band corresponds to a ring-twist motion of the linearly-arranged CH_2–CH_2–CH_2 fragment in the central diamine chelate ring. The related vibration of the **hc** conformer appears at 460 cm^{-1} in the spectrum of Li[Fe(tmdta)]·3H_2O (**1a**) and at 454 cm^{-1} in the scaled, computed spectrum of the geometry-optimized **hc** conformer (*cf.* band 26 in Fig. 2 (bottom) and Table 2). This vibration belongs to a rocking motion of the central methylene group in the diamine chelate ring. No significant Raman intensity is observed in the **tb** spectrum between 460 and 450 cm^{-1} (*cf.* Fig. 1). The most intense band in the 600–300 cm^{-1} region of the **hc** conformer appears at 480 cm^{-1} (*cf.* bands 27 and 28 in Fig. 2 (bottom) and Table 2). This feature is assigned to rocking motions of the axial glycinate rings, which are motions unique to this conformer.

The assignments of the remaining bands are presented in Table 1 and Table 2. The results show that the experimental and calculated

Table 2 Bands of the solid-state Raman spectrum of **1a** (**hc** conformer)

		Wavenumber/cm^{-1}			
No.	Sym.[a]	Exp'l[b]	Calc'd[c]	Intensity[d]	Description
24	A	408	404.6	8.9	Ring bend
25	A		414.9	5.0	Ring bend
26	A	459	453.6	5.2	Ring rock
27	A	483	474.5	7.3	Gly rock (ax1)
28	A		479.5	8.5	Gly rock (ax2)
29	A	516	500.7	4.6	ν(Fe–N_1) + ring twist
30	A	538	532.9	5.6	ring rock
31	A	544	549.1	4.1	ν(Fe–N_2) + ring twist

[a] Irreducible representation in the C_1 point group. [b] *cf.* Fig. 2, bottom. [c] Calculated wavenumbers scaled by a factor of 1.027. [d] Calculated Raman intensity.

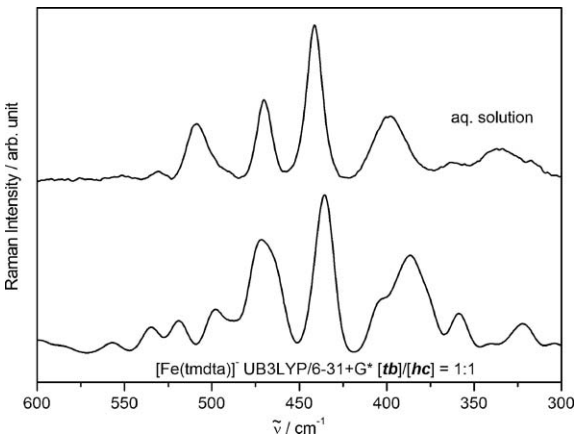

Fig. 3 Comparison of the unique Raman spectrum of aqueous solutions of **1a–e** and a computed spectrum generated by mixing pure computed **hc** and **tb** spectra in the ratio 1 : 1. Calculated wavenumbers are scaled by a factor of 1.012.

Raman spectra for the **hc** and **tb** conformers agree reasonably well. Deviations in vibrational energies might be due to (a) solid-state packing effects (size difference between counter-cations), (b) electrostatic interactions of the metal-bound and free carboxylato oxygen atoms of tmdta^{4-} with counter-cations and (c) hydrogen bonds between these oxygens and protons of the crystal water molecules. All of these might affect the vibrational energies.

It can therefore be concluded that differences between the Raman spectra of the two conformers in the 500–400 cm^{-1} range represent a crucial tool that allows aqueous solutions of [Fe(tmdta)]$^-$ salts to be analysed in terms of being (i) a pure solution of either conformer or (ii) a mixture of both conformers. The decision between (i) and (ii), followed by quantification of a possible equilibrium, can thus be based on the absolute intensities of the Raman signals of each conformer. In order to achieve this, and to avoid the tedious calibration of experimental Raman spectra, we have used the calculated absolute Raman intensities of the different bands, which are obtained directly from calculated molecular polarizabilities by means of theoretical methods. Comparison of the calculated and experimental spectra shows a good agreement between the relative Raman intensities, justifying this approach. Thus, linear combinations of the calculated spectra of pure species with varying [**tb**]/[**hc**] ratios were generated until a best fit of the experimental solution spectrum with the theoretical composite spectrum was achieved.

Since the calculated energies of the **tb** and the **hc** conformers in the gas phase are nearly equal ($\Delta H_{\mathbf{hc}-\mathbf{tb}} = -0.13$ kJ mol^{-1}, $\Delta G_{\mathbf{hc}-\mathbf{tb}} = 0.54$ kJ mol^{-1}), and since their calculated dipole moments ($\mu_{\mathbf{hc}} = 10.56$ Debye, $\mu_{\mathbf{tb}} = 10.54$ Debye) suggest a nearly identical electrostatic contribution to their free solvation energy, one would expect a [**tb**]/[**hc**] ratio of about 1 : 1 in aqueous solutions of [Fe(tmdta)]$^-$ on the basis of DFT calculations.

Fig. 3 shows the simulated spectrum that gives the best agreement with the experimental solution spectrum. In fact, this is the theoretical composite Raman spectrum with a 1 : 1 [**tb**]/[**hc**] ratio, as predicted by thermodynamic considerations. Importantly, with the help of the band assignments obtained for the pure conformers, it is now possible to fully understand the solution spectrum and to interpret the solution as an *equal* mixture of both forms. The most intense band near 440 cm^{-1} in the simulated solution spectrum (Fig. 3) corresponds to vibration **tb** 26 (ring twist), slightly broadened by the less intense band **hc** 26 (ring rock). The band at 470 cm^{-1} is a mixture of **tb** bands 28 and 29 (Fe–N stretch), and **hc** features 27 and 28 (gly rock). The remaining broad bands above 500 and below 400 cm^{-1} are mixtures of various normal modes of both conformers. Thus, the spectrum of the 1 : 1 [**tb**]/[**hc**] equilibrium mixture in the 600–300 cm^{-1} region is dominated by contributions of the **tb** conformer because of its more intense Raman vibrations. However, the presence of the band at 470 cm^{-1} clearly indicates the presence of the **hc** conformer at a significant concentration; in a pure **tb** solution spectrum, the band next to the ring twist would be expected to occur at a higher wavenumber (around 500 cm^{-1}).

This report is the first demonstration of how the combined application of Raman spectroscopy and quantum chemical methods can be used to quantify the equilibrium species involved in the interconversion of labile coordination isomers. The two new crystal structures of the [Fe^{III}(tmdta)]$^-$ salts, **1d** (inorganic counter-cation) and **1e** (organic counter-cation), reveal that the **tb** conformation is generally preferred in the solid-state. The detailed vibrational band assignments obtained for the Raman spectra of pure solids of both conformers allowed a revision of the previously incorrectly determined [**tb**]/[**hc**] ratio[8] of aqueous [Fe^{III}(tmdta)]$^-$ solutions, where the **hc** fraction was assumed to be present in a large excess. On the contrary, our analysis of the Raman spectrum of [Fe(tmdta)]$^-$ in aqueous solution reveals a [**tb**]/[**hc**] ratio of about 1 : 1. We are currently investigating the mechanistic details of the [**tb**]/[**hc**] interconversion and the possible influence of the [Fe^{III}(tmdta)]$^-$ water exchange reaction on the dynamics of this process. Furthermore, work is in progress to apply our approach of DFT-supported Raman studies to elucidation of the dynamics in solution of related metal–tmdta complexes in order to evaluate the role of the central metal ion in the conformational equilibrium.

Notes and references

‡ Coordinates for the structures of four monomeric complexes have been deposited with the CCDC. Deposition numbers: CCDC 649049 (**1a**), 649050 (**1b**), 649047 (**1d**) and 649048 (**1e**). For crystallographic data in CIF or other electronic format see DOI: 10.1039/b708437d

§ We are grateful to N. Burzlaff (Erlangen) for solving the X-ray structure of **1b**.

1 R. Meier, *Habilitation Thesis*, University of Leipzig, Leipzig, 2003.
2 W. L. Howard and D. A. Wilson, Chelating Agents, in *Kirk–Othmer Encyclopedia of Chemical Technology*, ed. J. I. Kroschwitz and M. Howe-Grant, John Wiley & Sons, New York, 4th edn, 1993, vol. **5**, pp. 764–795.
3 T. Egli, *J. Biosci. Bioeng.*, 2001, **92**, 89; C. K. Schmidt and H.-J. Brauch, Aminopolycarboxylate Complexing Agents in *Organic Pollutants in the Water Cycle*, ed. T. Reemtsma and M. Jekel, Wiley-VCH, 2006, pp. 155–180.
4 T. Yamamoto, K. Mikata, K. Miyoshi and H. Yoneda, *Inorg. Chim. Acta*, 1988, **150**, 237.
5 H. P. Bommeli, G. Anderegg and W. Petter, *Z. Kristallogr.*, 1986, **174**, 23; H. P. Bommeli, *Dissertation Thesis*, ETH Zürich, Zürich, 1992.
6 K.-I. Okamoto, K. Kanamori and J. Hikada, *Acta Crystallogr., Sect. C: Cryst. Struct. Commun.*, 1990, **46**, 1640.
7 K. Kanamori, H. Dohniwa, N. Ukita, I. Kanesaka and K. Kawai, *Bull. Chem. Soc. Jpn.*, 1990, **63**, 1447.
8 K. Kanamori, N. Ukita, K. Kawai, S. Taguchi, K. Goto, T. Eguchi and M. Kishita, *Inorg. Chim. Acta*, 1991, **186**, 205.
9 Crystallographic data and refinement details of **1a**, **1b**, **1d** and **1e** are summarized in Table S1. Important bond lengths and angles are given in Table S2‡.